

Gate-tunable strong-weak localization transition in few-layer black phosphorus

Gen Long,¹ Shuigang Xu,¹ Xiangbin Cai,¹ Zefei Wu,¹ Tianyi Han,¹ Jiangxiazhi Lin,¹ Yuanwei Wang,¹ Liheng An,¹ Yuan Cai,¹ Xinran Wang,² and Ning Wang^{1,*}

¹*Department of Physics and Center for Quantum Materials,
the Hong Kong University of Science and Technology, Hong Kong, China*

²*National Laboratory of Solid State Microstructures, School of Electronic Science and Engineering,
and Collaborative Innovation Center of Advanced Microstructures, Nanjing University, Nanjing 210093, China*

(Dated: March 28, 2017)

Atomically thin black phosphorus (BP) field-effect transistors show strong-weak localization transition which is tunable through gate voltages. Hopping transports through charge impurity induced localized states are measured at low-carrier density regime. Variable-range hopping model is applied to simulate the charge carrier scattering behavior. In the high-carrier concentration regime, a negative magnetoresistance signals the weak localization effect. The extracted phase coherence length is power-law temperature dependent ($\sim T^{-0.48 \pm 0.03}$) and demonstrates electron-electron interactions in few-layer BP. The competition between the Strong localization length and phase coherence length is proposed and discussed based on the observed gate tunable strong-weak localization transition in few-layer BP.

Keywords: Black phosphorus; Strong localization; Weak localization; electron-electron interaction; Variable-range hopping

Atomically thin two-dimensional (2D) materials, such as graphene and transition metal dichalcogenides have opened new avenues for exploring physical property anomalies and potential applications in nanoelectronics and optoelectronics [1–16]. Single- or few-layer black phosphorus (BP) [14–19] is another promising 2D material characterized by high mobility at room temperature, a tunable direct band gap, and high in-plane anisotropy properties for both the fundamental study of thermal, optical, and optoelectronics properties and technological applications [4, 20–22]. Recently, interesting Shubnikov de Haas oscillations and quantum Hall effects have been demonstrated in boron nitride (BN)-encapsulated few-layer BP high-mobility field-effect transistors (FETs) at cryogenic temperatures [23–28]. However, achieving ultrahigh mobility BP FETs at low carrier density remains a challenge in the further study of a number of intriguing physics properties, such as many-body phenomena or fraction quantum Hall effects.

We discuss here an experimental study of the charge carrier scattering behaviors in few-layer BP at various charge carrier densities, temperatures, and magnetic fields. We found that at low-carrier concentration regime ($\sim 10^{11} \text{ cm}^{-2}$), strong localization is on account of low-carrier mobility of a few $\text{cm}^2 \text{ V}^{-1} \text{ s}^{-1}$ and the observed localization effects can be fitted by the variable-range hopping (VRH) model for low temperature region [29]. Meanwhile, at high-carrier concentration ($\sim 10^{12} \text{ cm}^{-2}$), weak localization occurs and a high carrier mobility of up to $10^3 \text{ cm}^2 \text{ V}^{-1} \text{ s}^{-1}$ is achieved. We discuss the mechanisms for gate-tunable strong-weak localization transition by extracting the phase coherence lengths and inelastic scattering time in high-carrier concentrations [30].

Our few-layer BP FETs are fabricated using exfoliated BP flakes. The quality of BP flakes degrades

in atmospheric conditions due primarily to oxidation. To avoid BP quality degradation, few-layer BP samples are encapsulated between two hexagonal BN (h-BN) sheets to form h-BN/BP/h-BN encapsulation structures [23, 24, 27, 28, 31]. The exfoliation and encapsulation processes are performed in a glove box filled with nitrogen to protect the exfoliated BP flakes (more details regarding the device-fabrication process are available in the Method section).

Figure 1a shows the variation of BP channel conductance for different gate voltages at 1.8 K. The red arrow indicates the charge neutrality point (CNP) obtained from the linear fitting of the charge carrier versus the gate voltage (Fig. 1c). The charge carrier concentrations shown in Fig. 1c are determined by Hall effect measurement. The vertical dashed lines in Fig. 1a divide the transport curve into three distinguishable regions. In region I (adjacent to CNP), the carrier mobility ranges within a few $\text{cm}^2 \text{ V}^{-1} \text{ s}^{-1}$. A high mobility of approximately $2000 \text{ cm}^2 \text{ V}^{-1} \text{ s}^{-1}$ is achieved in region III (high-carrier concentration), indicating different charge carrier scattering behaviors at different carrier concentrations in our BP FETs. The transition between the two different scattering behaviors occurs in region II.

To further explore the different charge carriers scattering behaviors, we measured the temperature T dependences of channel conductance G for different gate voltages as shown in Fig. 1b. For low-carrier concentrations ($V_g > -5 \text{ V}$), decreasing the temperature strongly influences channel conductance when the temperature surpasses 100 K. On the other hand, the impact of temperature on channel conductance is much smaller for temperatures lower than 40 K. These temperature-dependence features of channel conductance indicate strong localizations induced by charge impurities for low-carrier concen-

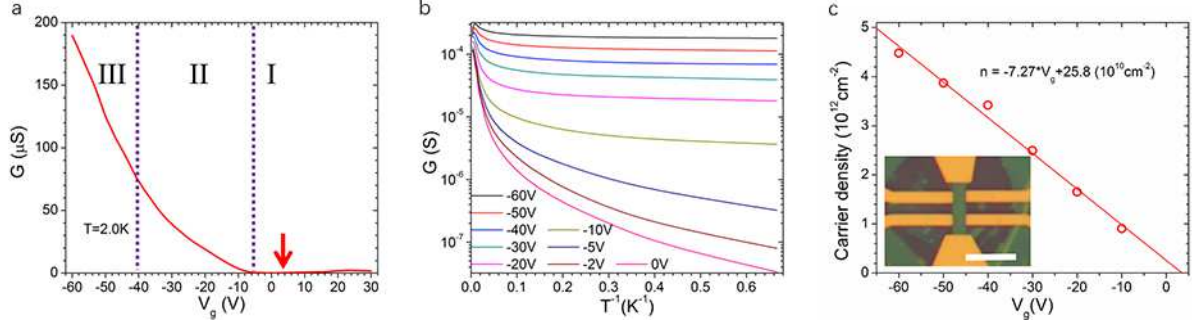


FIG. 1. **Carrier concentrations and temperatures dependence of channel performances.** (a) Four-terminal transfer curve at $T=1.8\text{K}$. The red arrow indicates the charge neutral point (threshold gate voltage). The two vertical dashed lines divide the transfer curve into three different regions. (b) Arrhenius plot of channel conductance. (c) Carrier density obtained from Hall effect as a function of gate voltages. The inset shows an optical image of a typical device. Scale bar: $10\mu\text{m}$

trations in our devices. For high-carrier concentrations ($V_g < -40\text{V}$), the channel conductance shows a weak dependence on temperature, and the magnetic resistance of our devices shows typically weak localization features. To further confirm the claimed gate-tunable strongweak localization transition in few-layer BP, the charge-carrier scattering behaviors are simulated by VRH, and Hikami-Larkin-Nagaoka (HLN) models at low- and high-carrier concentrations.

STRONG LOCALIZATION AT LOW-CARRIER CONCENTRATIONS ($\sim 10^{11}\text{cm}^{-2}$)

Figure 2a shows the channel resistance plotted as a function of $T^{1/3}$ at low-carrier concentrations at temperatures ranging from 1.8 K to 40 K. The linear dependence of $\log R$ vs. $T^{1/3}$ perfectly fits the 2D VRH model:

$$R \propto \exp\left(\frac{T_0}{T}\right)^{\frac{1}{2+1}}$$

where T_0 is the characteristic temperature [32]. The gate voltage dependence of T_0 (Fig. 2b) agrees with the VRH model and serves as the signature of hopping transport via localized states [10, 33]. The localization length ξ_{VRH} can be extracted from $\xi_{VRH} = \sqrt{\frac{13.8}{k_B \rho(E) T_0}}$, where T_0 is the characteristic temperature obtained from the VRH model and $\rho(E)$ is the density of state (DOS) at the Fermi level [34]. The DOS of the two dimensional hole gas can be expressed as $\rho(E) = \frac{m^*}{\pi \hbar^2}$, where $m^* = 0.26m_0$ is the effective mass of holes. The calculated gate voltage dependence of ξ_{VRH} is shown in Fig. 2b. ξ_{VRH} increases as the gate voltage decreases (increasing the carrier concentration), a pattern that is widely observed in two dimensional electron systems [33, 35]. The increasing trend of ξ_{VRH} can be explained by the two dimensional hydrogen atom model. The high energy states are occupied when the density of the localized charge carriers increases, resulting in two dimensional hydrogen atoms with a large

radius (localization length). From another perspective, the increasing localization length may also be explained by the screening effect, as the localized charge carriers screen the electronic field of the localization center and thus contribute to a weak localization strength, i.e., large localization length [10, 36].

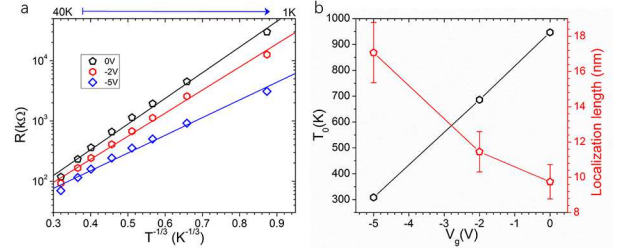


FIG. 2. **Variable-range hopping at low temperature.** (a) Channel resistances as functions of $T^{-1/3}$ for different gate voltages (carrier concentrations). The solid lines show the fitting results of variable-range hopping model. (b) T_0 and localization lengths obtained from the fitting results.

As temperature increases, the resistance deviates from the 2D VRH model and fits to the Arrhenius behavior $R \propto \exp(\frac{T_1}{T})$ as shown in Fig. S1a (Supplementary materials), where T_1 is the characteristic temperature which reflects excitation energy. Normally, the linear dependence of $\log R$ on T^{-1} signals the crossover from VRH to nearest neighbor Hopping model. However in our device, the excitation energy extracted from the fitting results is quite small (Fig. S1b, Supplementary materials) which is lower than the physical temperature. The scattering process is rather dominated by the high-temperature incoherence diffusive transport than nearest neighbor hopping [37].

WEAK LOCALIZATION AT HIGH-CARRIER CONCENTRATIONS ($\sim 10^{12} \text{cm}^{-2}$)

As carrier concentration further increases, the dependence of the channel resistance on temperature becomes increasingly weak (Fig. 1b). The VRH model fails to describe the variation of the channel resistance after entering region II (Fig. 1a). To explore the transport behavior of charge carriers in the high-carrier concentration regime ($\sim 10^{12} \text{cm}^{-2}$), we measured the magneto-conductance of our samples under different gate voltages and temperatures (Figs. 3a and b). The applied perpendicular magnetic field leads to a positive magneto-conductance (negative magneto-resistance), which is consistent with the features of weak localization [38–40]. The weak localization is a quantum correction to the conductance of a diffusive system originating from the phase interference of charge carrier wave functions. For a 2D electron system with a zero Berry phase ϕ , the wave functions of backscattered charge carriers would have constructive interference, which increases the probability of backscattering. Thus, weak localization generally induces a negative quantum correction to the channel conductance. The applied perpendicular magnetic field induces extra changes to ϕ , which break the constructive interference of backscattering and consequently lead to the positive magneto-conductance. The weak localization is strongly carrier-concentration dependent. In the present case, the magneto-conductance increases with the increasing carrier concentration (Fig. 3a). When the temperature is lower than 2 K, the weak localization is weakly temperature dependent. The magneto-conductance will decrease with increasing temperature when $T > 2 \text{K}$. To further explore the carrier concentration and temperature dependences of weak localization, we simulate the measured magneto-conductance with the HLN model:

$$\delta\sigma = \sigma(B) - \sigma(B=0) = \frac{e^2}{\pi h} \left[\Psi\left(\frac{1}{2} + \frac{B_\phi}{B}\right) - \ln\left(\frac{B_\phi}{B}\right) \right]$$

where σ is the device conductivity; h is the Planck constant; and e is the elemental charge. Ψ refers to the digamma function. $B_\phi = \frac{\hbar}{4eL_\phi^2}$ is the phase coherence magnetic field, and L_ϕ is the phase coherence length [41–43]. The green solid lines in Figs. 3a and b represent the carrier concentration and temperature fitting results, respectively, of the HLN model. The HLN model reproduces the experimental features of magneto-conductance between 0.4 and 0.4 T, especially the deep dips at zero magnetic field.

Figure 4a displays the temperature dependence of L_ϕ for various gate voltages. A maximum L_ϕ of 202 nm is obtained at $T = 1.4 \text{K}$ and $V_g = -60 \text{V}$. For temperatures lower than 2 K, L_ϕ exhibits weak dependence on temperature. We fit L_ϕ with a powerlaw formula $L_\phi \propto T^{-\beta}$ from 2.3 K to 40 K. A universal $\beta = 0.48 \pm 0.03$ for different

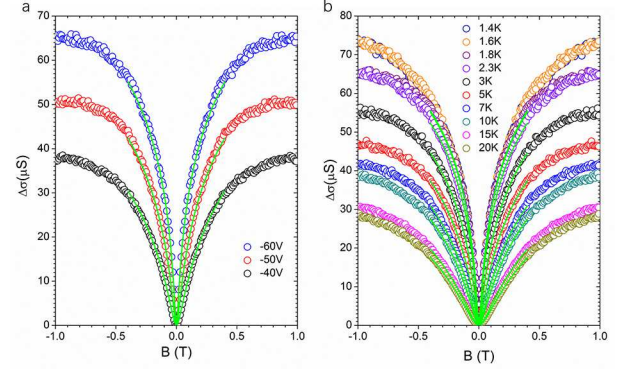


FIG. 3. **Weak localization at high carrier concentrations.** (a) and (b) Normalized conductivity $\delta\sigma$ as functions of magnetic fields for different gate voltages at $T = 1.8 \text{K}$, and for different temperatures with a fixed gate voltage of $V_g = -60 \text{V}$, respectively. The green solid lines show the fitting results of Hikami-Larkin-Nagaoka (HLN) model.

gate voltages is obtained from the fitting results. Specifically, the temperature dependence of inelastic scattering time $\tau_\phi = \frac{L_\phi^2}{D} \propto T^{-\alpha}$ distinguishes different scattering mechanisms, where $\alpha = 2\beta$ and $D = \frac{\sigma \pi \hbar^2}{m^* e^2}$ is the diffusion constant. τ_ϕ is determined to be 5.3 ps at $T = 1.4 \text{K}$ and $V_g = -60 \text{V}$. The linear dependence of τ_ϕ^{-1} on T as shown in Fig. 4b demonstrates that $\alpha = 1$, which is consistent with the obtained β value. The inelastic electronic interactions with small momentum transfer can be described by the Altshuler Aronov Khmelnitsky theory $\tau_\phi = \frac{\hbar}{k_B T} \frac{h\sigma/e^2}{\ln(h\sigma/e^2)}$, and the linear dependence of τ_ϕ^{-1} on T can be expected from the theory considering channel conductance as independent on temperature. The observed deviation of β from 0.5 can be explained by the temperature dependence of σ [41]. The gate voltage (or carrier concentration) dependence of L_ϕ is depicted in Fig. 4c, and L_ϕ decreases with decreasing carrier concentration. This decrease of L_ϕ can be ascribed to the carrier-concentration dependence of σ .

The observed gate tunable strong/weak localization transition can be ascribed to the competition between L_ϕ and ξ_{VRH} . At low-carrier concentrations, $\xi_{VRH} < L_\phi$ leads to a suppression of the interference of electronic wave functions, and strong localization dominates the weak localization caused by electronelectron interactions [37, 44, 45]. As carrier concentrations increase, ξ_{VRH} increases and reaches $\xi_{VRH} > L_\phi$ at high-carrier concentrations. In this case, the electronic wave function interference plays the leading role in the charge-carrier scattering processes, and strong localization is suppressed [37, 44, 45]. While, in region II (Fig. 1a), both strong and weak localizations influence the transport properties of the BP samples.

This study probed distinguishable charge-carrier transport behaviors for varying carrier concentrations in few-

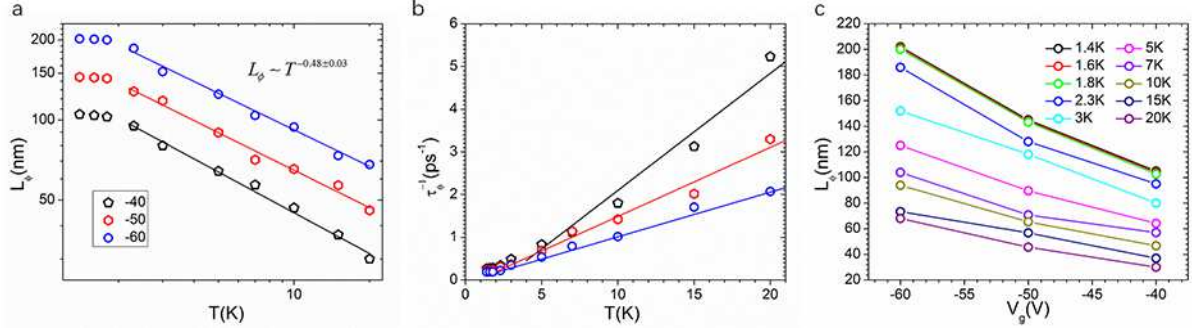


FIG. 4. **Phase coherence lengths L_ϕ and inelastic scattering time τ_ϕ obtained from Hikami-Larkin-Nagaoka (HLN) model.** (a) L_ϕ depends on temperatures at different gate voltages. (b) τ_ϕ^{-1} linearly depends on temperatures for different gate voltages. (c) L_ϕ depend on gate voltages at varying temperatures.

layer BP. Strong and weak localization models are proposed to simulate charge-carrier scattering behavior for low- and high-carrier concentrations, respectively. The strong localization is confirmed by the observation of VRH at low temperatures. The weak localization model is confirmed by the magneto-transport features. A competition behavior between strong localization length and phase coherence length is proposed to occur on account of the gate-tunable strongweak localization transition.

Method

Few-layer BP and h-BN thin films are exfoliated from the bulk crystals on heavily doped silicon substrates covered with 300 nm thick SiO_2 . Another h-BN flake is simultaneously prepared on the poly(methyl methacrylate) (PMMA) thin film. The h-BN flake on the PMMA film is used to pick up the BP flakes, and the formed h-BN/BP structure is then placed on the h-BN flakes on a silicon substrate. The h-BN/BP/h-BN heterostructure is then constructed. All these processes are performed in an inert gas environment to minimize the degradation of BP quality. This method avoids the direct contact between the PMMA film and BP flakes. Annealing at 300°C in Ar flow for 10 h is applied to further stabilize the heterostructure.

Reaction-ion etching (RIE) (recipe: 4 sccm O_2 + 40 sccm CHF_3 ; RF power: 200 W) after the electron beam lithography (EBL) is used to define the Hall structures. A selective RIE etching is then applied to etch the top h-BN at the contact areas defined by the second EBL. The third EBL is then used to define the contact metal patterns followed by the electron beam evaporation to deposit the contact metals (Cr/Au=5/60 nm).

Electrical measurements are performed with the lock-in technique in a cryogenic system under low pressure.

Acknowledgements

We acknowledge the helpful discussion with Prof. Sheng. Financial support from the Research Grants Council of Hong Kong (Project Nos. 16302215, HKU9/CRF/13G, 604112, and N_HKUST613/12) and technical support of

the Raith-HKUST Nanotechnology Laboratory for the electron-beam lithography facility at MCPF are hereby acknowledged.

Competing financial interests

The authors declare no competing financial interests.

Author contributions

G. Long and N. Wang conceived the project. G. Long fabricated the devices and performed cryogenic measurements with the help of S. Xu. G. Long, X. Wang and N. Wang analyzed the data and wrote the manuscript. Other authors provided technical assistance in the project.

* Correspondence to: phwang@ust.hk

- [1] K. Novoselov, D. Jiang, F. Schedin, T. Booth, V. Khotkevich, S. Morozov, and A. Geim, Proceedings of the National Academy of Sciences of the United States of America **102**, 10451 (2005).
- [2] A. C. Neto, F. Guinea, N. M. Peres, K. S. Novoselov, and A. K. Geim, Reviews of modern physics **81**, 109 (2009).
- [3] A. K. Geim, science **324**, 1530 (2009).
- [4] A. A. Balandin, S. Ghosh, W. Bao, I. Calizo, D. Teweldebrhan, F. Miao, and C. N. Lau, Nano letters **8**, 902 (2008).
- [5] L. Mattheiss, Physical Review B **8**, 3719 (1973).
- [6] J. Wilson and A. Yoffe, Advances in Physics **18**, 193 (1969).
- [7] A. Ayari, E. Cobas, O. Ogundadegbe, and M. S. Fuhrer, Journal of applied physics **101**, 014507 (2007).
- [8] Z. Yu, Z.-Y. Ong, Y. Pan, Y. Cui, R. Xin, Y. Shi, B. Wang, Y. Wu, T. Chen, Y.-W. Zhang, *et al.*, Advanced Materials **28**, 547 (2016).
- [9] Y. Cui, R. Xin, Z. Yu, Y. Pan, Z.-Y. Ong, X. Wei, J. Wang, H. Nan, Z. Ni, Y. Wu, *et al.*, Advanced Materials **27**, 5230 (2015).
- [10] H. Qiu, T. Xu, Z. Wang, W. Ren, H. Nan, Z. Ni, Q. Chen, S. Yuan, F. Miao, F. Song, *et al.*, Nature communications **4** (2013).
- [11] H. Qiu, L. Pan, Z. Yao, J. Li, Y. Shi, *et al.*, Applied Physics Letters **100**, 123104 (2012).

- [12] K. F. Mak, C. Lee, J. Hone, J. Shan, and T. F. Heinz, *Physical Review Letters* **105**, 136805 (2010).
- [13] G. Long, S. Xu, T. Zhang, Z. Wu, W. K. Wong, T. Han, J. Lin, Y. Cai, and N. Wang, *Applied Physics Letters* **109**, 183107 (2016).
- [14] L. Li, Y. Yu, G. J. Ye, Q. Ge, X. Ou, H. Wu, D. Feng, X. H. Chen, and Y. Zhang, *Nature nanotechnology* **9**, 372 (2014).
- [15] F. Xia, H. Wang, and Y. Jia, *Nature communications* **5** (2014).
- [16] J. Qiao, X. Kong, Z.-X. Hu, F. Yang, and W. Ji, *Nature communications* **5** (2014).
- [17] A. Castellanos-Gomez, L. Vicarelli, E. Prada, J. O. Island, K. Narasimha-Acharya, S. I. Blanter, D. J. Groenendijk, M. Buscema, G. A. Steele, J. Alvarez, *et al.*, *2D Materials* **1**, 025001 (2014).
- [18] Y. Takao, H. Asahina, and A. Morita, *Journal of the Physical Society of Japan* **50**, 3362 (1981).
- [19] X. Ling, H. Wang, S. Huang, F. Xia, and M. S. Dresselhaus, *Proceedings of the National Academy of Sciences* **112**, 4523 (2015).
- [20] H. Yuan, X. Liu, F. Afshinmanesh, W. Li, G. Xu, J. Sun, B. Lian, A. G. Curto, G. Ye, Y. Hikita, *et al.*, *Nature nanotechnology* **10**, 707 (2015).
- [21] M. Buscema, D. J. Groenendijk, G. A. Steele, H. S. Van Der Zant, and A. Castellanos-Gomez, *Nature communications* **5** (2014).
- [22] X. Wang, A. M. Jones, K. L. Seyler, V. Tran, Y. Jia, H. Zhao, H. Wang, L. Yang, X. Xu, and F. Xia, *Nature nanotechnology* **10**, 517 (2015).
- [23] N. Gillgren, D. Wickramaratne, Y. Shi, T. Espiritu, J. Yang, J. Hu, J. Wei, X. Liu, Z. Mao, K. Watanabe, *et al.*, *2D Materials* **2**, 011001 (2014).
- [24] G. Long, S. Xu, J. Shen, J. Hou, Z. Wu, T. Han, J. Lin, W. K. Wong, Y. Cai, R. Lortz, *et al.*, *2D Materials* **3**, 031001 (2016).
- [25] L. Li, G. J. Ye, V. Tran, R. Fei, G. Chen, H. Wang, J. Wang, K. Watanabe, T. Taniguchi, L. Yang, *et al.*, *Nature nanotechnology* **10**, 608 (2015).
- [26] V. Tayari, N. Hemsworth, I. Fakihi, A. Favron, E. Gaufrès, G. Gervais, R. Martel, and T. Szkopek, *Nature communications* **6** (2015).
- [27] L. Li, F. Yang, G. J. Ye, Z. Zhang, Z. Zhu, W. Lou, X. Zhou, L. Li, K. Watanabe, T. Taniguchi, *et al.*, *Nature nanotechnology* (2016).
- [28] G. Long, D. Maryenko, J. Shen, S. Xu, J. Hou, Z. Wu, W. K. Wong, T. Han, J. Lin, Y. Cai, *et al.*, *Nano Letters* (2016).
- [29] R. Abou-Chakra, D. Thouless, and P. Anderson, *Journal of Physics C: Solid State Physics* **6**, 1734 (1973).
- [30] B. Altshuler, D. Khmel'Nitzkii, A. Larkin, and P. Lee, *Physical Review B* **22**, 5142 (1980).
- [31] X. Chen, Y. Wu, Z. Wu, Y. Han, S. Xu, L. Wang, W. Ye, T. Han, Y. He, Y. Cai, *et al.*, *Nature communications* **6** (2015).
- [32] R. Hill, *Physica status solidi (a)* **34**, 601 (1976).
- [33] M. Y. Han, J. C. Brant, and P. Kim, *Physical review letters* **104**, 056801 (2010).
- [34] W. Li, Y. He, L. Wang, G. Ding, Z.-Q. Zhang, R. W. Lortz, P. Sheng, and N. Wang, *Physical Review B* **84**, 045431 (2011).
- [35] Z. Yu and X. Song, *Physical Review Letters* **86**, 6018 (2001).
- [36] F. Van Keuls, X. Hu, H. Jiang, and A. Dahm, *Physical Review B* **56**, 1161 (1997).
- [37] M. Gershenson, Y. B. Khavin, D. Reuter, P. Schafmeister, and A. Wieck, *Physical review letters* **85**, 1718 (2000).
- [38] M. P. Van Albada and A. Lagendijk, *Physical review letters* **55**, 2692 (1985).
- [39] Y. Du, A. T. Neal, H. Zhou, and D. Y. Peide, *2D Materials* **3**, 024003 (2016).
- [40] Y. Shi, N. Gillgren, T. Espiritu, S. Tran, J. Yang, K. Watanabe, T. Taniguchi, and C. N. Lau, *2D Materials* **3**, 034003 (2016).
- [41] B. L. Altshuler, A. Aronov, and D. Khmelnitsky, *Journal of Physics C: Solid State Physics* **15**, 7367 (1982).
- [42] G. Bergmann, *Physics Reports* **107**, 1 (1984).
- [43] S. Hikami, A. I. Larkin, and Y. Nagaoka, *Progress of Theoretical Physics* **63**, 707 (1980).
- [44] J. Moser, H. Tao, S. Roche, F. Alzina, C. S. Torres, and A. Bachtold, *Physical Review B* **81**, 205445 (2010).
- [45] B. R. Matis, F. A. Bulat, A. L. Friedman, B. H. Houston, and J. W. Baldwin, *Physical Review B* **85**, 195437 (2012).